

UNCLASSIFIED

AD NUMBER

ADB026143

LIMITATION CHANGES

TO:

Approved for public release; distribution is unlimited.

FROM:

Distribution authorized to U.S. Gov't. agencies only; Test and Evaluation; OCT 1977. Other requests shall be referred to Air Force Materials Lab., Wright-Patterson AFB, OH 45433.

AUTHORITY

AFWAL ltr 21 Sep 1982

THIS PAGE IS UNCLASSIFIED

L

2
B.S.

AFML-TR-77-212

AD B026143

CHARACTERIZATION OF REACTION SINTERED SILICON NITRIDE RADOMES

*PROCESSING AND HIGH TEMPERATURE MATERIALS BRANCH
METALS AND CERAMICS DIVISION*

OCTOBER 1977

TECHNICAL REPORT AFML-TR-77-212
Final Report for Period 1 January 1977 - 1 September 1977

DDC
APR 10 1978
A

AD No. _____
DDC FILE COPY

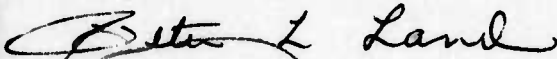
Distribution limited to U. S. Government agencies only; test and evaluation; September 1977. Other requests for this document must be referred to the Air Force Materials Laboratory, Metals and Ceramics Division, Processing and High Temperature Materials Branch, AFML/LLM, or to the Electromagnetic Materials Division, Laser Hardened Materials Branch, AFML/LPJ, Wright-Patterson Air Force Base, Ohio 45433.

AIR FORCE MATERIALS LABORATORY
AIR FORCE WRIGHT AERONAUTICAL LABORATORIES
AIR FORCE SYSTEMS COMMAND
WRIGHT-PATTERSON AIR FORCE BASE, OHIO 45433

NOTICE

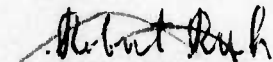
When Government drawings, specifications, or other data are used for any purpose other than in connection with a definitely related Government procurement operation, the United States Government thereby incurs no responsibility nor any obligation whatsoever; and the fact that the government may have formulated, furnished, or in any way supplied the said drawings, specifications, or other data, is not to be regarded by implication or otherwise as in any manner licensing the holder or any other person or corporation, or conveying any rights or permission to manufacture, use, or sell any patented invention that may in any way be related thereto.

This technical report has been reviewed and is approved for publication.



PETER L. LAND

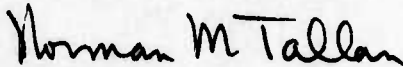
Processing and High Temperature Materials Branch



ROBERT RUH

Processing and High Temperature Materials Branch

FOR THE COMMANDER



NORMAN M. TALLAN

Chief, Processing and High Temperature
Materials Branch

Metals and Ceramics Division

Air Force Materials Laboratory

Copies of this report should not be returned unless return is required by security considerations, contractual obligations, or notice on a specific document.

UNCLASSIFIED

SECURITY CLASSIFICATION OF THIS PAGE (When Data Entered)

REPORT DOCUMENTATION PAGE		READ INSTRUCTIONS BEFORE COMPLETING FORM	
1. REPORT NUMBER AFML-TR-77-212	2. GOVT ACCESSION NO.	3. RECIPIENT'S CATALOG NUMBER	(9)
4. TITLE (and Subtitle) Characterization of Reaction Sintered Silicon Nitride Radomes.		5. TYPE OF REPORT & PERIOD COVERED Final Report, 1 Jan 1977 - 1 Sep 1977,	
7. AUTHOR(s) P.L. LAND R. RUH		8. CONTRACT OR GRANT NUMBER(s)	
9. PERFORMING ORGANIZATION NAME AND ADDRESS Air Force Materials Laboratory (LLM) AF Wright Aeronautical Laboratories, AFSC Wright-Patterson Air Force Base, Ohio 45433		10. PROGRAM ELEMENT, PROJECT, TASK AREA & WORK UNIT NUMBERS 61102F 2306-202 62102F 2422-401	
11. CONTROLLING OFFICE NAME AND ADDRESS		12. REPORT DATE October 1977	
14. MONITORING AGENCY NAME & ADDRESS (if different from Controlling Office) (12) 49p. (17) P2, 04		13. NUMBER OF PAGES 49	
16. DISTRIBUTION STATEMENT (of this Report) Distribution limited to U.S. Government agencies only; test and evaluation; Sep 77. Other requests for this document must be referred to the Air Force Materials Laboratory, Metals and Ceramics Division, Processing and High Temperature Materials Branch, AFML/LLM, or to the Electromagnetic Materials Division, Laser Hardened Materials Branch, AFML/LPJ, WPAFB OH 45433.		15. SECURITY CLASS. (of this report) UNCLASSIFIED	
17. DISTRIBUTION STATEMENT (of the abstract entered in Block 20, if different from Report)		15a. DECLASSIFICATION/DOWNGRADING SCHEDULE	
18. SUPPLEMENTARY NOTES			
19. KEY WORDS (Continue on reverse side if necessary and identify by block number) Radome, Reaction Bonded Silicon Nitride			
20. ABSTRACT (Continue on reverse side if necessary and identify by block number) This report describes the observations and characterization of reaction-sintered silicon nitride radomes produced by Raytheon Corporation for the Air Force. The radomes were tested at NASA-Ames with a CO ₂ laser and failed under less stringent conditions than expected. Portions of the radomes removed for flexure specimens had extensive flawed areas consisting of many voids of approximately 100 micron diameter. The strength and bulk density of the flexure specimens ranged from 12,000 to 18,000 psi and from 2.1 to 2.2 gm/cm ³ which is substantially lower (SEE ATTACHED)			

DD FORM 1 JAN 73 1473 EDITION OF 1 NOV 65 IS OBSOLETE

UNCLASSIFIED

SECURITY CLASSIFICATION OF THIS PAGE (When Data Entered)

012 320

LB

UNCLASSIFIED

SECURITY CLASSIFICATION OF THIS PAGE(When Data Entered)

than the values anticipated by Raytheon, approximately 25,000 psi and 2.35 - 2.6 gm/cm. Most of the flaws identified as fracture origins in the AFML flexure specimens consisted of one or two voids about 100 microns in diameter. The fractures under laser irradiation may have initiated at one of the large defects (S) 500 microns in diameter - which are present on the fracture surface near the periphery of the irradiated region. Since tensile strength decreases with the inverse square root of the linear dimension of the flaws in a homogeneous material, it is estimated that the radomes may have fractured at stress levels below 8,000 psi. Several thermal stress models for laser irradiation of ceramic radome materials were reviewed; none specifically addressed the failure mode which may have occurred in the radomes. It is suggested that (stress matrices) recently calculated by Martin Marietta Corporation for finite element models of plane and spherical discs of silicon nitride be diagonalized in order to determine the surface of maximum tensile stress which would determine the zone of probable fracture initiation versus time. The possibility of pre-catastrophic cracking is discussed, and the possibly different dependences of fracture modes on material properties such as thermal diffusivity is noted.

UNCLASSIFIED

SECURITY CLASSIFICATION OF THIS PAGE(When Data Entered)

FOREWORD

This work was conducted under Task 2422, work unit 24220401 of AFML/LPJ and Task 2306, work unit 2306P202 of AFML/LLM, and accomplished in the Processing and High Temperature Materials Branch, Metals and Ceramics Division, Air Force Materials Laboratory, Air Force Wright Aeronautical Laboratories.

The authors gratefully acknowledge the optical photography by Mr. B.F. Schreiber of the University of Dayton (UD), the SEM photos by Mr. A.T. Biermann of UD, the strength measurements by Mr. R.F. Klinger of Systems Research Laboratories, Inc., the x-radiography by Mr. J.E. Porter of Universal Technologies Corp., impurity analyses by Mr. J.H. Muntz of AFML/TUA, and helpful discussions of the fracture of ceramics under complex stress states with Dr. M.G. Mendiratta of Systems Research Laboratories, Inc., and with Mr. J.R. Koenig of AFML/LC.

ACQUISITION FOR	
NTIS	Write Section <input type="checkbox"/>
DDC	Buff Section <input checked="" type="checkbox"/>
UNANNOUNCED	<input type="checkbox"/>
JUSTIFICATION	
BY	
RESTRICTION/AVAILABILITY CODES	
1st	2nd or SPECIAL
β	

TABLE OF CONTENTS

SECTION		PAGE
I	INTRODUCTION	1
II	EXPERIMENTAL RESULTS	2-31
	1. Observations on Tested Radomes	2
	2. Flexure Samples from Radomes	9
	a. Preparation	9
	b. Fabrication Flaws	9
	c. Nondestructive Evaluation	12
	d. Density	12
	3. Flexure Strength	14
	4. Fractography of Flexure Samples	17
	5. Characterization of Material	26
	a. Microstructure and Energy Dispersion Analysis by X-Rays (EDAX)	26
	b. X-Ray Diffraction (XRD)	26
	c. Chemical Analysis	26
	d. Discussion	30
III	CONCLUSIONS AND RECOMMENDATIONS	32
IV	REFERENCES	34
	APPENDIX A - THERMAL STRESS ANALYSIS	36

LIST OF ILLUSTRATIONS

FIGURE	PAGE
1. The fracture surface of Radome 1, (a) 4X, (b) 0.5X. The arrows indicate flaws that could have initiated fracture.	3
2. The fracture surface of Radome 2. (a) 3.5X, (b) 0.4X. The arrows indicate flaws that could have initiated fracture.	4
3. The fracture surface of Radome 3. (a) 6X, (b) 0.5X. The arrows indicate flaws that could have initiated fracture.	5
4. The fracture surface of Radome 4. (a) 1X, (b) 0.7X. The arrows indicate flaws that could have initiated fracture.	6
5. The fracture surface of Radome 5. (a) 8X, (b) 0.6X. The arrows indicate flaws that could have initiated fracture.	7
6. A drawing showing how flexure specimens were removed from the radomes.	10
7. (a) A side view of a typical flexure bar from Radome 5. (b) A flawed area of the tensile surface of sample 3-4b. (c) A scanning electron micrograph of the edge of sample 3-4b showing that the flaw is three dimensional.	11
8. (a) A radiograph of the flexure bars from Radome 3 through the tensile and compression surface.(b) A radiograph of the flexure bars from Radome 5 through the perpendicular to the tensile and compression surface.	13
9. The fracture surface (a) and tensile surface (b) of flexure bar 3-2A.	18
10. The fracture surface (a) and tensile surface (b) of flexure bar 3-3B.	19
11. The fracture surface (a) and tensile surface (b) of flexure bar 3-4A.	20
12. The fracture surface (a) and tensile surface (b) of flexure bar 3-4B.	21
13. The fracture surface (a) and tensile surface (b) of flexure bar 3-5A.	22
14. The fracture surface (a) and tensile surface (b) of flexure bar 3-5B.	23

FIGURE	PAGE
15. The fracture surface (a) and tensile surface (b) of flexure bar 5-1A.	24
16. The fracture surface (a) and tensile surface (b) of flexure bar 5-1B.	25
17. A secondary emission scanning electron micrograph of a sample from Radome 3. (a) 2000X, (b) 500X, (c) 15X. Circled areas EDAX alike.	27
18. (a) A secondary emission scanning electron micrograph of a polished sample from Radome 3 at 20X. (b) An EDAX scan for silicon concentration of the same area.	28
19. An EDAX trace from a polished sample of Radome 3. (a) The peaks from left to right correspond to Al, Si, Au, Pd, and Fe. The Au and Pd are from the conductive coating. (b), (c), (d) Lines superimposed on the peaks of (a) identify peaks belonging to Al, Si and Fe.	29
A1 - The coordinates and stress matrix for the MM models of Si_3N_4 discs.	
A2 - (a) The isotherms for a 0.3 inch thick disc of Si_3N_4 with a 1.56 inch diameter hot spot applied for 2.0 seconds, as calculated from Martin Marietta's Figure 35. (b) The limits of locally induced shear stress and shear strain for the above figure and the equivalent tensile stress-strain.	

SECTION I

INTRODUCTION

This report describes properties of Raytheon reaction-sintered silicon-nitride radomes produced under AFML/LPJ Contract F33615-74-C-5160, managed by Mr. D.J. Evans. Five radomes were tested for resistance to CO₂ laser damage at NASA-Ames under the direction of Dr. W. Laughlin of AFWL. It was concluded that the radomes failed under less stringent conditions than they should have if the domes had the expected strength. Therefore, AFML/LLM was asked to investigate the mechanical properties of the domes.

The work done includes fractography of the domes and of flexure samples cut from the domes, observation of fabrication flaws, flexure strength measurements, density determinations, phase and impurity analysis, optical and SEM microstructural analysis, and inspection by x-radiography and ultrasonic C-scan. A discussion of thermal fracture and mathematical modeling of laser induced thermal stress is included in the appendix.

SECTION II

EXPERIMENTAL RESULTS AND DISCUSSION

1. OBSERVATIONS ON TESTED RADOMES

Figures 1 through 5 show views of the upper portion of five fractured radomes. On each fracture surface there are flaws which are large compared to the 100 to 200 micron flaws which were the sites of initial fracture in flexure bars used to measure the strength of the radome material. These large flaws, which could have initiated fracture, include internal voids and inclusions, extended regions where the prefracture bond strength across the fractured surface was apparently weaker than in the bulk, and large chips, cracks and laminations on the inner surface.

The origins of fracture are not clear since fracture mirrors and associated features which often permit unequivocal identification of a fracture origin were not observed. There are, however, ridges radiating to the outer surface from flawed areas which may be an indication that fracture initiated at the neighboring flawed area. The small pieces of material recovered from the wind tunnel were inspected for fracture mirrors and other markings, but nothing significant was found.

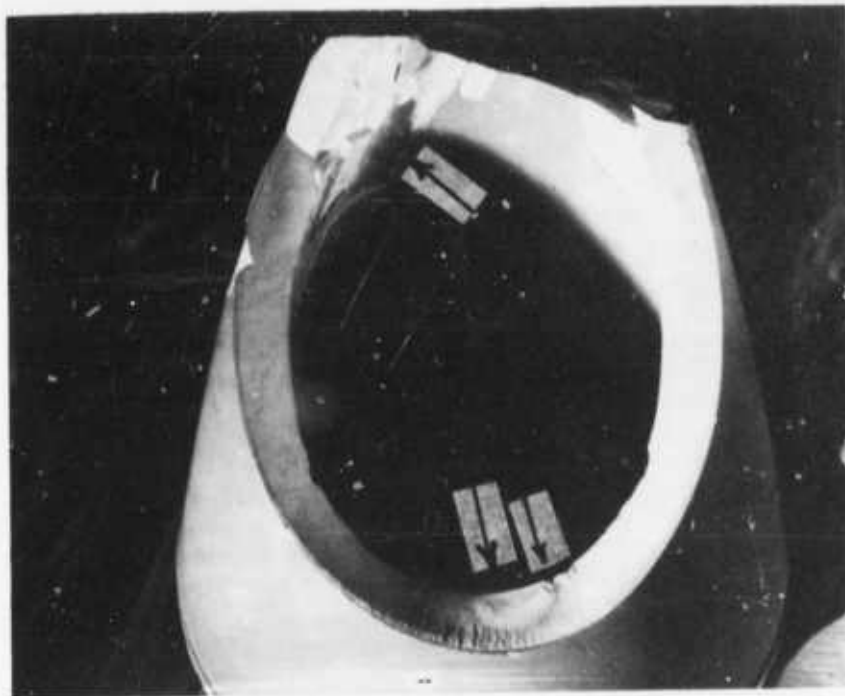
The elliptical shaped holes in the domes are approximately the same size and shape as the area heated by the laser beam. The predominant inclination of the fracture surfaces is outward from the normal to the radome wall, particularly in the area nearest the base of the radome.

The relation relating the strength, σ , of a material and the size, a , of strength limiting flaws such as cracks or voids is

$$\sigma \propto \sqrt{a}$$



(a)

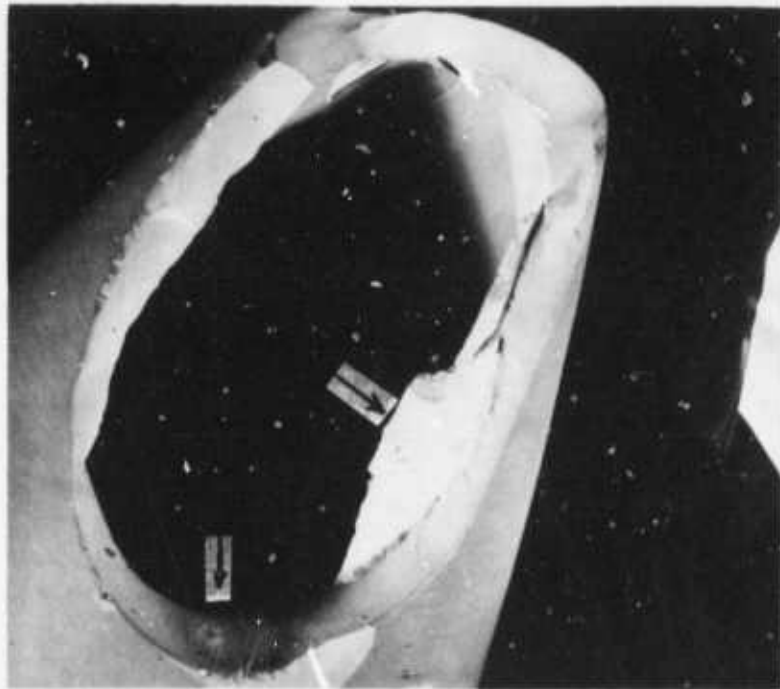


(b)

Figure 1. The fracture surface of Radome 1. (a) 4X. (b) 0.5X. The arrows indicate flaws that could have initiated fracture.

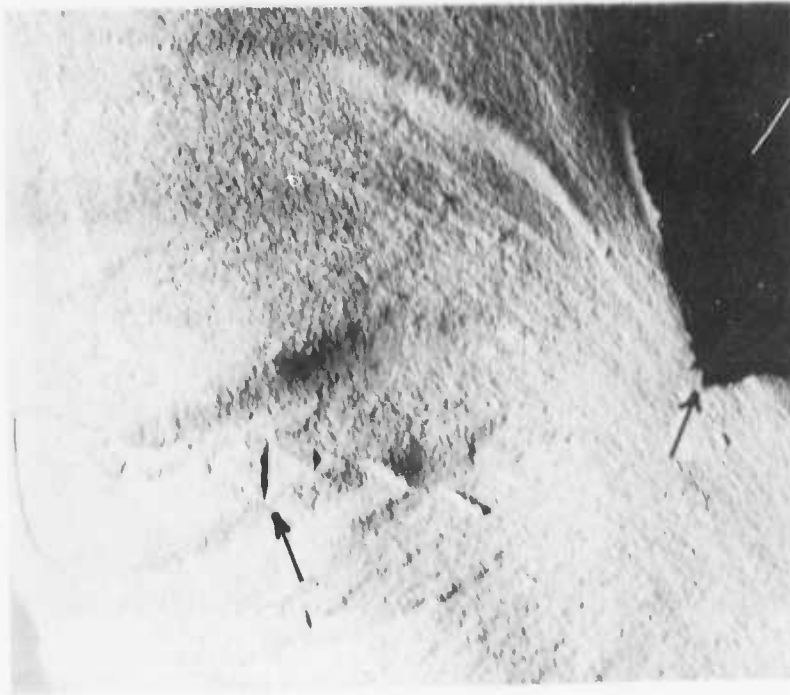


(a)

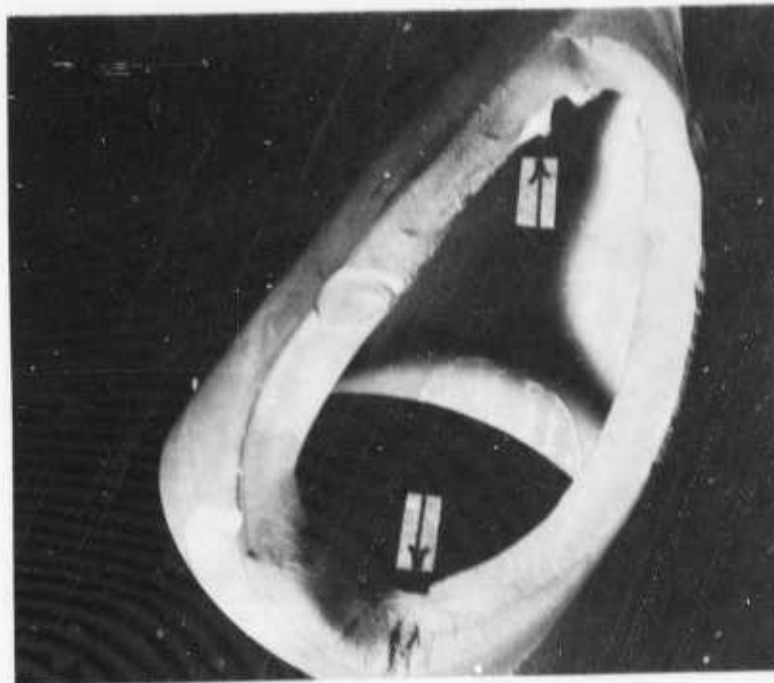


(b)

Figure 2. The fracture surface of Radome 2. (a) 3.5X. (b) 0.4X. The arrows indicate flaws that could have initiated fracture.

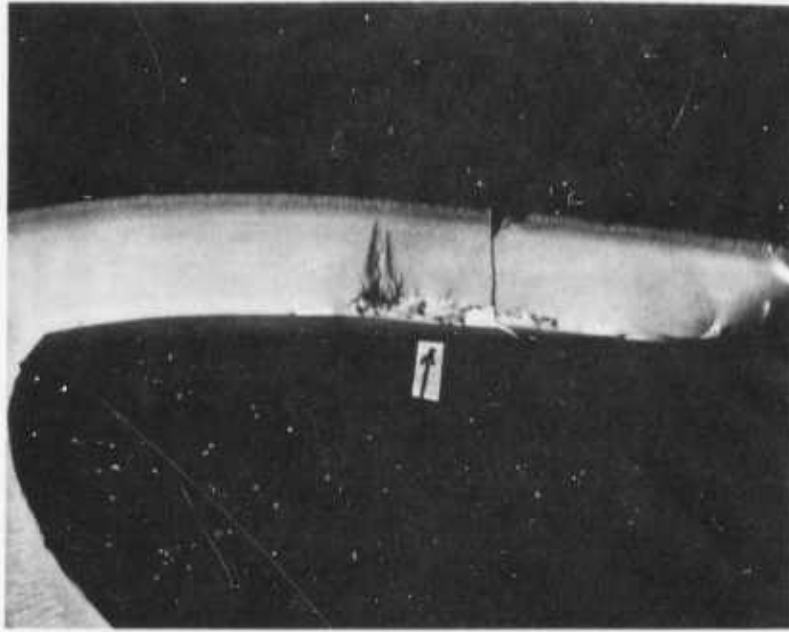


(a)

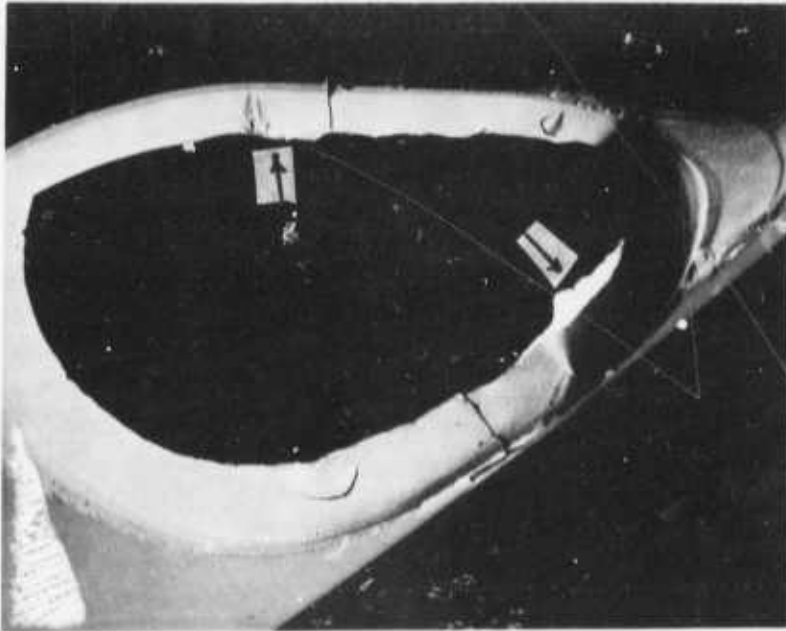


(b)

Figure 3. The fracture surface of Radome 3. (a) 6X. (b) 0.5X. The arrows indicate flaws that could have initiated fracture.

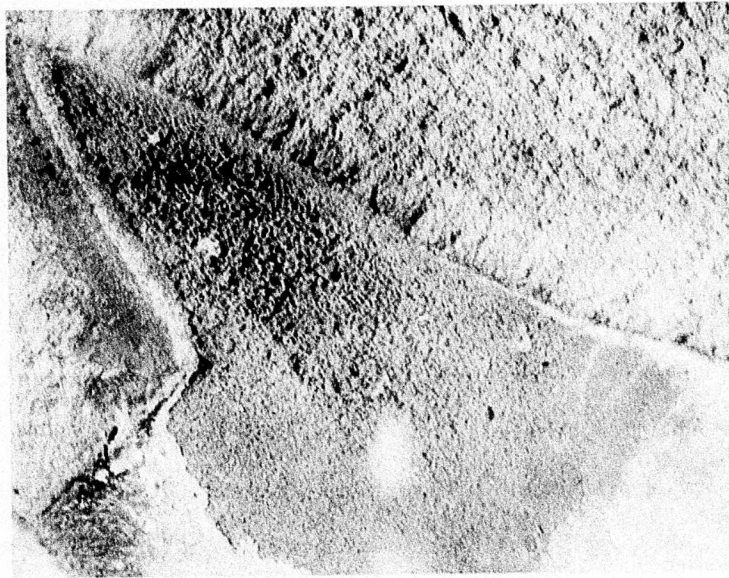


(a)

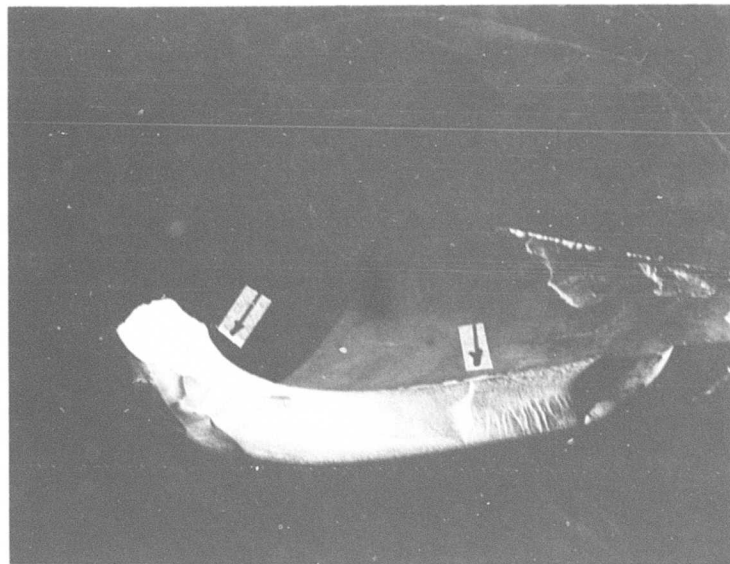


(b)

Figure 4. The fracture surface of Radome 4. (a) 1.0X. (b) 0.7X. The arrows indicate flaws that could have initiated fracture.



(a)



(b)

Figure 5. The fracture surface of Radome 5. (a) 8X. (b) 0.6X. The arrows indicate flaws that could have initiated fracture.

The chipped areas and cracks in the inner surface and the inclusion and voids in the interior of the radome which are revealed by the fracture are more than 5 times the size of the critical flaws observed in the flexure bars. This suggests that the tensile strength of the radomes may be less than half of the average value indicated by flexure measurements. The above equation does not, of course, relate the strength and size of flaws having different prefracture bond strength across the flaw. Therefore, it is not possible to estimate the effect on strength of inclusions or extended flaws such as the lightly shaded regions of lower than average-density material.

It is well known that strength decreases with increasing stressed volume because of the increased probability of having a critical flaw. In addition, recent work has indicated that different flaw populations may contribute to fracture when the stressed volume are substantially different^{1,2}. Therefore strength measurements on flexure bars, which provide small stressed volume and which may be basically different because of the difference in fabrication may have limited value in predicting the stress that a radome will withstand.

2. FLEXURE SAMPLES FROM RADOMES

a. Preparation

Test samples were diamond machined from Radomes 3 and 5 since these radomes had the longest and shortest survival time, respectively. Figure 6 is a sketch showing where test material was removed to make 2.375 in. by 0.25 in. by 0.25 in. four-point bend specimens for strength measurements. The tensile surfaces of samples labeled A are the original outer surface and those labeled B are from the approximate center of the radome wall. This sampling is considered sufficient since Raytheon tested material from 4 sectors and from the top, middle, and base area of one radome and found no difference associated with location.

b. Fabrication Flaws

After the bars were cut to 1/4 in. sq. cross section size, it was observed that both radomes had a zone of porosity just beneath the surface. This can be seen in Figure 7a. In addition, an area of Radome 3 contained extended flaws which were revealed as 0.1 mm size pores in the sectioned pieces. This can be seen in Figure 7b and c. The worst flaws occurred in Sections 2, 4 and 5 of Radome 3. The three-dimensional continuity of the flaws is illustrated by an edge view of sample 3-4B, (Figure 7c). The fracture surface of 3-4A, Figure 11, shows a hump and valley where the fracture passes through a weak zone. The hump and depression have pullouts and matching voids which are about the same size as the 0.1mm pores in the surface of the bars. This suggests that some of the exposed pores were not initially void, but that poorly bonded material was detached during the cutting operation.

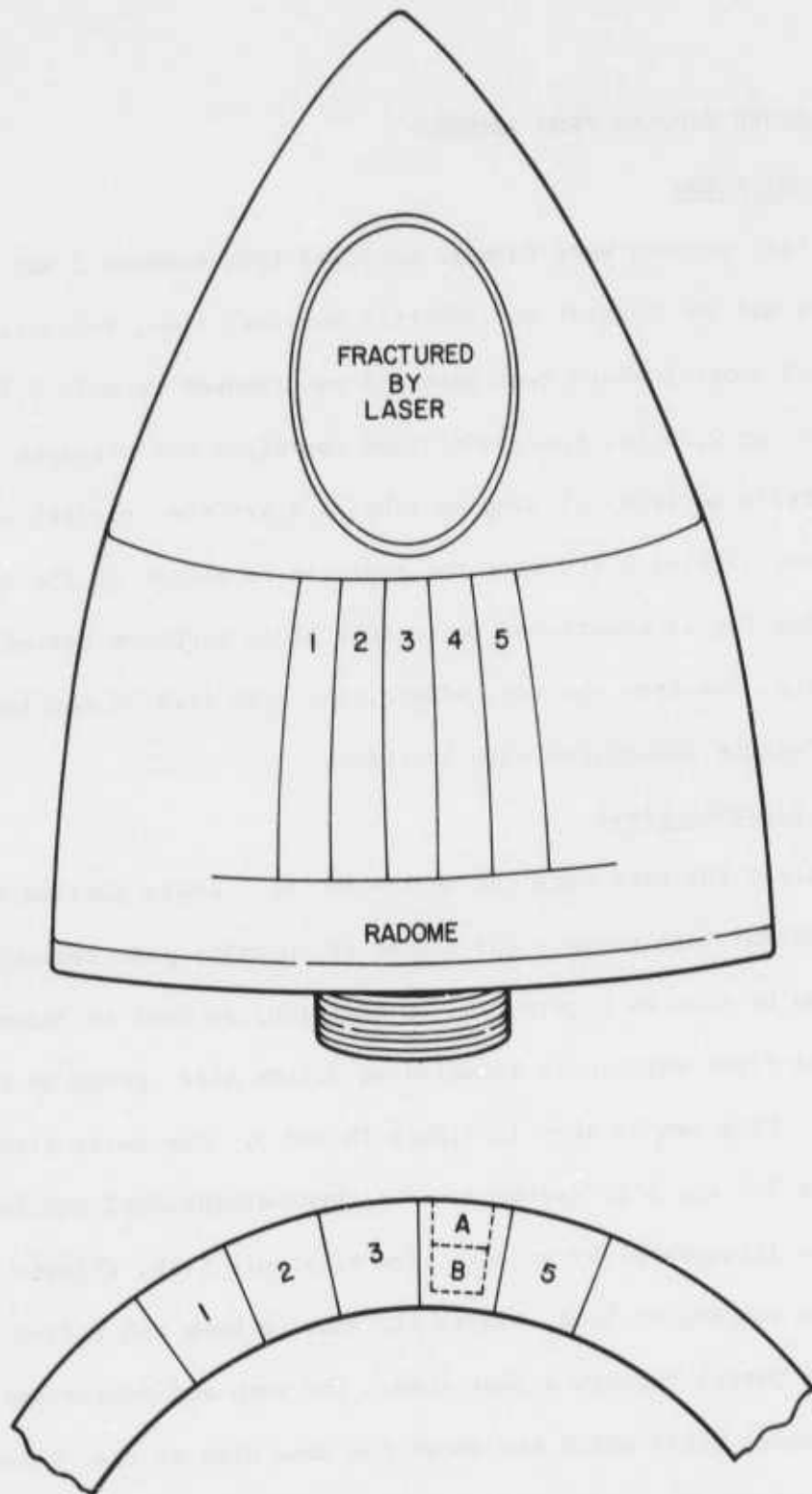


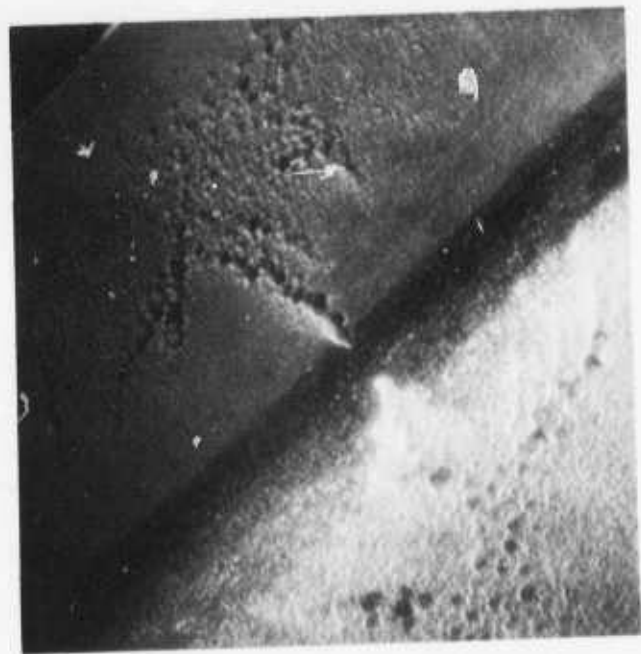
Figure 6. A drawing showing how flexure specimens were removed from the radomes.



(a)



(b)



(c)

Figure 7. (a) A side view of a typical flexure bar from Radome 5. (b) A flawed area of the tensile surface of sample 3-4B. (c) A scanning electron micrograph of the edge of sample 3-4B showing that the flaw is three dimensional.

c. Nondestructive Evaluation (NDE)

Before the bars were cut from the radome, the radome was coated with fluorescent-dye penetrant and inspected under ultraviolet light. No cracks or other flaws were observed. Following the observation of extensive 0.1mm porosity in the surface of the test bars, all of the bars were x-rayed. Figure 8a shows variation in bulk density. Figure 8b shows the band of porosity just beneath the radome surface, and adjacent thin layers having slightly higher than average density. No feature was seen that corresponds to the extensive flaws indicated by the 0.1mm pores in the bar surfaces. The bars were subsequently inspected by microfocus x-ray and ultrasonic C-scan at AiResearch Corporation. A preliminary report indicated some inhomogeneity, but no features which correlate with the linked 0.1 mm pores in the surfaces of the bars.

d. Density

The bulk density of the bars ranged from 2.11 to 2.18 gm/cm³. This is somewhat lower than the 2.35 - 2.59 gm/cm³ reported by Raytheon (page 103)³. There was no consistent trend toward higher density in either the inner or outer set of bars. Apparently the porous material just beneath the surface is compensated by an adjacent denser bands of material. Raytheon reported that the effect of porosity on strength and modulus was such that a density of 2.2 to 2.4 gm/cm³ was desired for resistance to thermally induced fracture. They also noted that increased porosity reduces the dielectric constant.

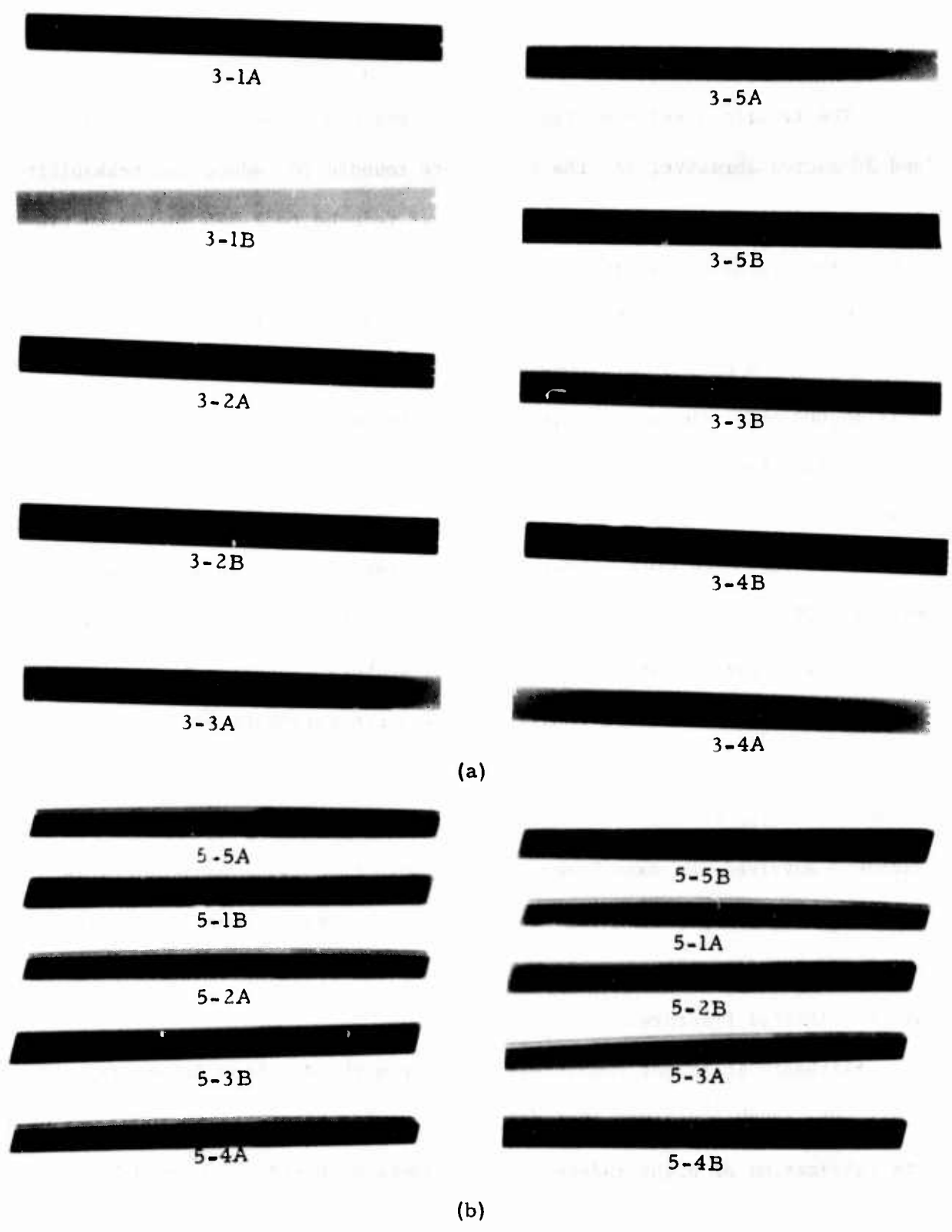


Figure 8.(a) A radiograph of the flexure bars from Radome 3 through the tensile and compression surface. (b) A radiograph of the flexure bars from Radome 5 through the perpendicular to the tensile and compression surface.

3. FLEXURE STRENGTH

The tensile surface of the bend bars was ground down successively by 70 and 30 micron abrasive, and the edges were rounded to reduce the probability of edge-initiated fracture. The length was reduced to 2.375 inches to fit a bend fixture having an inner span of 1 inch and an outer span of 2 inches.

The results of the bend tests are given in Table I. The average strength of the bars from Radome 3 is 16,000 psi while that for Radome 5 is 15,000 psi. The average strength of the outer surface is 1,000 psi greater than the interior, probably because this tensile surface was curved, or possibly because of a difference in density. The table shows that pores at the surface of the bars from Radome³ cause fracture initiation at stress levels as much as 30% less than that for similar, sounder bars. Two of the bars from Radome 5 were particularly weak, and their weakness appeared to be a bulk property rather than a result of stress concentration by localized flaws. The average strength of Radome 3 is slightly greater than that of Radome 5, so the relative strengths do not correlate with the fact that Radome 5 survived the same laser flux for more than twice as long. This is not particularly surprising since the failure stress depends upon the stress intensification or weakness caused by the specific critical flaw which initiated fracture.

Although it is not completely clear from the Raytheon Report (pp. 73 and 100),³ Dr. Waugh confirmed that dry milled powder batch SN6153-19D-0 was used in the fabrication of eight radomes. The radomes numbered 1-3 were 0.25 inch thick and those numbered 4-8 were 0.6 inches thick. Those numbered 4-8 were later numbered 1-5 by AFWL. The strength reported by Raytheon for test material taken from powder batch SN6153-19D-0 ranged from 23,000 to 30,000 psi with a mean value of 26,000 psi. The density of material taken from various

locations in their Radome No. 1 ranged from 2.49 to 2.60 gm/cm³. It is of course well known that the strength of reaction bonded silicon nitride decreases with decreasing density and that density usually decreases with thickness. The mean density and strength of the flexure samples from Radomes 3 and 5 is 2.1 to 2.2 gm/cm³ and 15,000 to 16,000 psi which is consistent with the extrapolation of strength versus density data given on page 75 of the Raytheon report³.

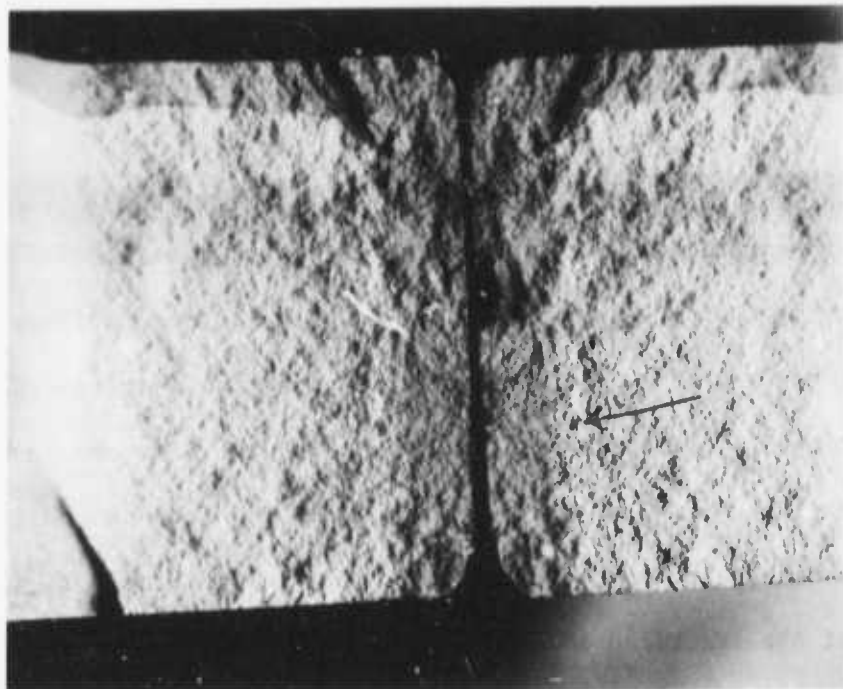
TABLE I
STRENGTH DATA FOR FOUR-PCINT BEND BARS

SAMPLE NO.	LOCATION OF FRACTURE	STRESS AT SURFACE (ksi)	REMARKS
3-1A	i	17.8	Fracture origin may be obscured by post-fracture damage; i.e. bar impact with bend fixture
3-1B	i	17.1	Fracture origin may be obscured by post-fracture damage; i.e., bar impact with bend fixture
3-2A	i	15.9	a
3-2B	i	16.8	b
3-3A	i	16.7	b
3-3B	i	16.1	a
3-4A	i	17.0	Fracture origin possibly an inclusion or surface damage. See photo.
3-4B	e	13.1	a
3-5A	i	14.5	a
3-5B	e	14.4	a
5-1A	i	16.7	Fracture origin at point of surface damage
5-1B	i	14.8	Photo of fracture surface shows pullouts;
5-2A	i	16.6	b
5-2B	e	15.9	b
5-3A	o	13.4	Fracture stress < 13.4 ksi (b)
5-3B	i	12.0	Fracture surface flat, as is typical for weak material (b)
5-4A	i	15.7	b
5-4B	i	15.4	b
5-5A	i	16.3	b
5-5B	i	16.0	b

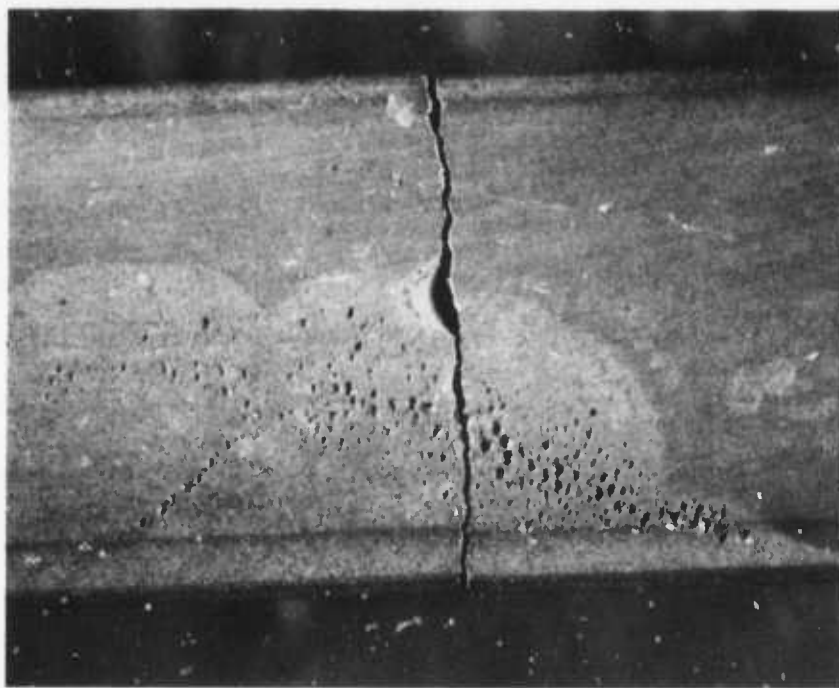
(a) Pores at a region of linked porosity cause fracture. (b) Fracture origin undetermined. (e) Fracture occurred at the end of the maximum stress region. (i) Fracture occurred within the maximum stress region. (o) Fracture occurred outside the maximum stress region.

4. FRACTOGRAPHY OF FLEXURE SAMPLES

Table I summarizes the observations of fracture surfaces. Figure 9-16 show the fracture surfaces and the flaws causing failure in those cases where the fracture origin is clearly indicated by the features of the fracture surface, i.e., by ridges radiating from the flaw and increasing smoothness near the flaw. The following statements are derived from observations of the fracture surfaces: (a) There are damaged regions near the center of the fractured tensile surface which are a result of post-fracture damage caused by the impact of the broken bar with a cylindrical part of the bend fixture. (b) Most of the identifiable fracture sources are pores in a zone of many 0.1mm pores. Two flaws, those in 3-4A (Fig. 11) and 5-1A, (Fig 15) may be a result of damage by cutting or grinding. (c) A large-scale pullout occurred in the fracture surface of 3-4A, Figure 11a, and within this region are small-scale pullout features which are comparable in size to the pores in the surfaces of the bend bars, ($\approx 0.1\text{mm}$). The pullouts are a result of below-average cohesion, and the region where they occur might be expected to yield a flawed surface if a diamond saw cut were made there. (d) The fracture surfaces of 5-3A and 5-3B, which were not photographed, are smoother than most others. This feature is indicative of low fracture energy and these were the bars with the lowest strength values.

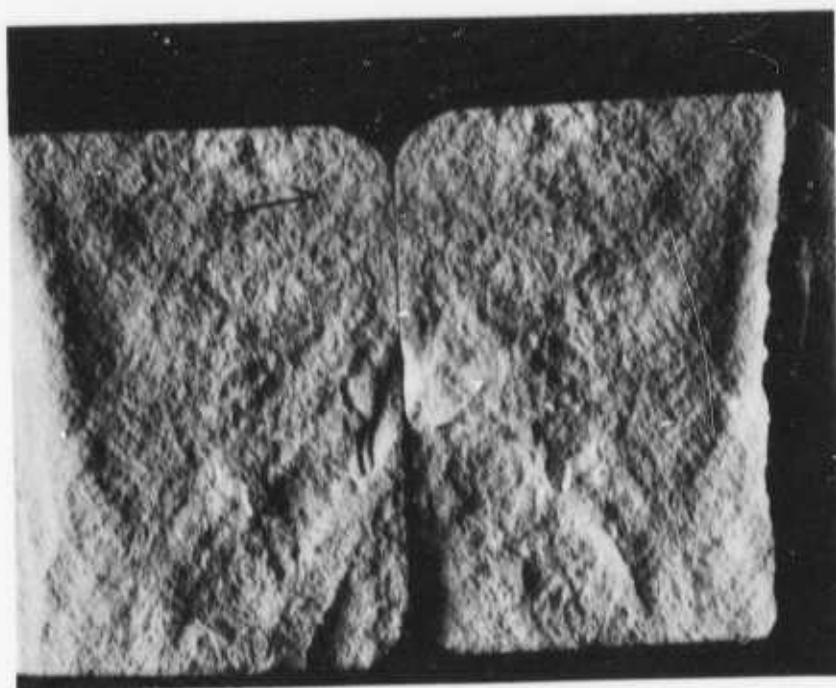


(a)



(b)

Figure 9. Fracture surface (a) and tensile surface (b) of flexure bar 3-2A.

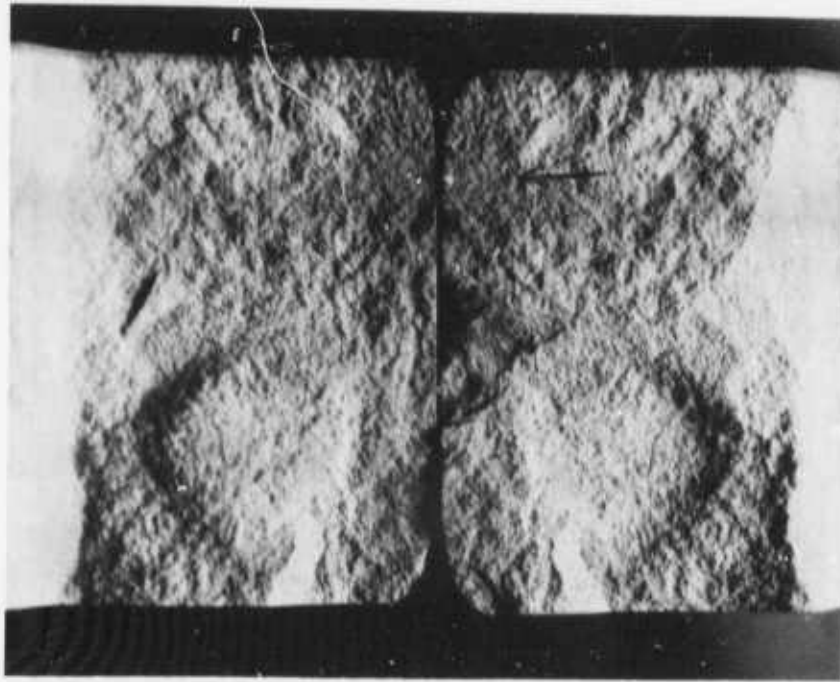


(a)

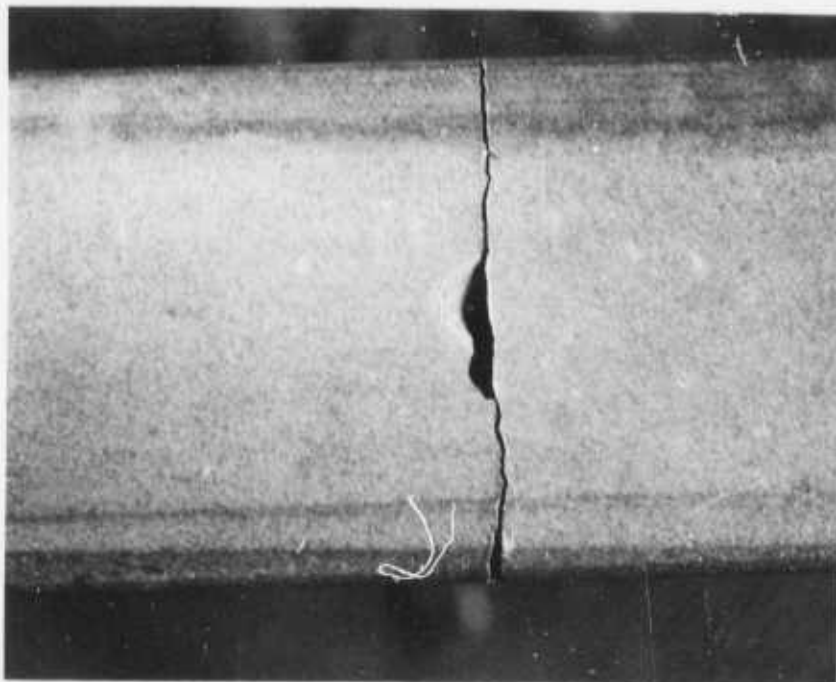


(b)

Figure 10. Fracture surface (a) and tensile surface (b) of flexure bar 3-3B.

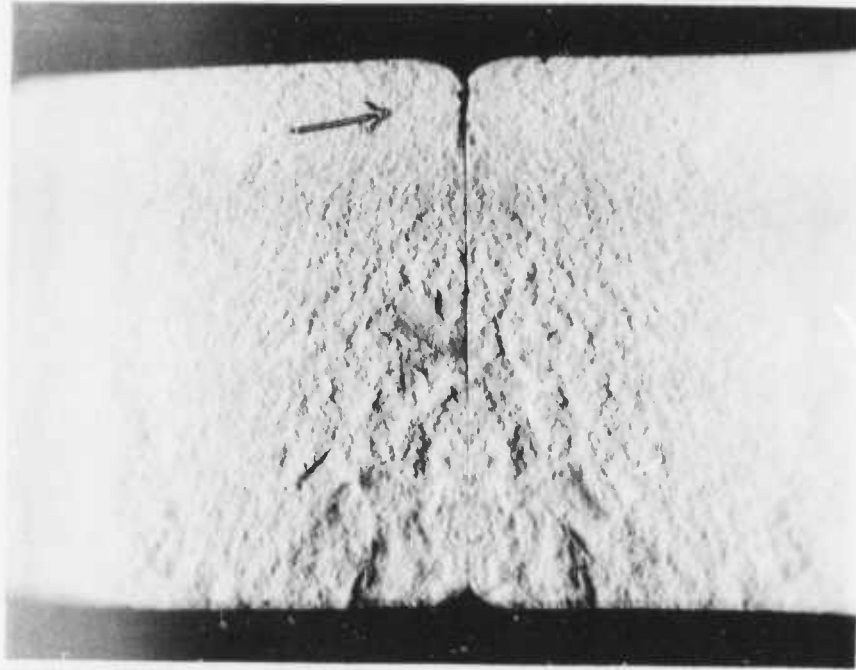


(a)

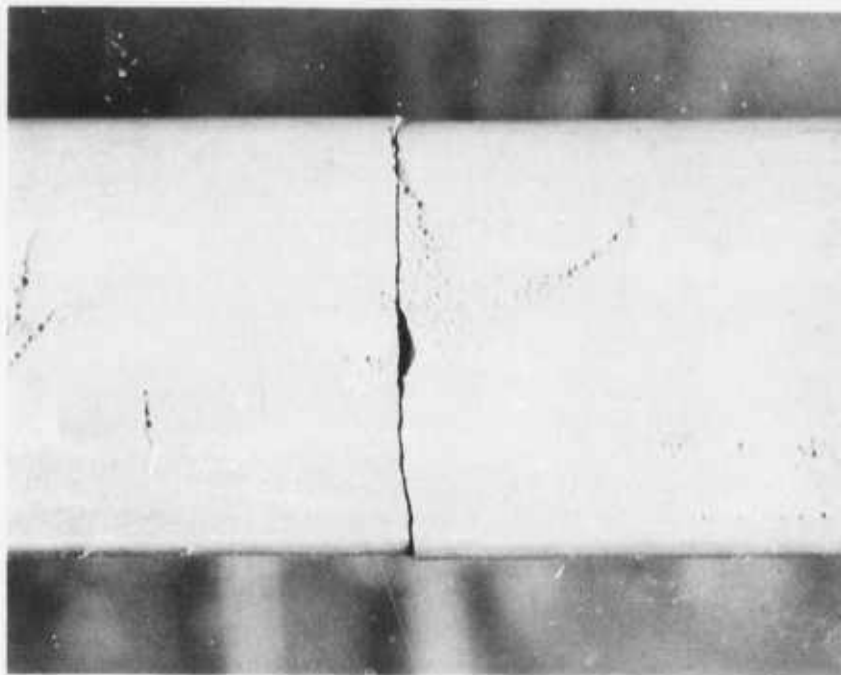


(b)

Figure 11. Fracture surface (a) and tensile surface (b) of flexure bar 3-4A.

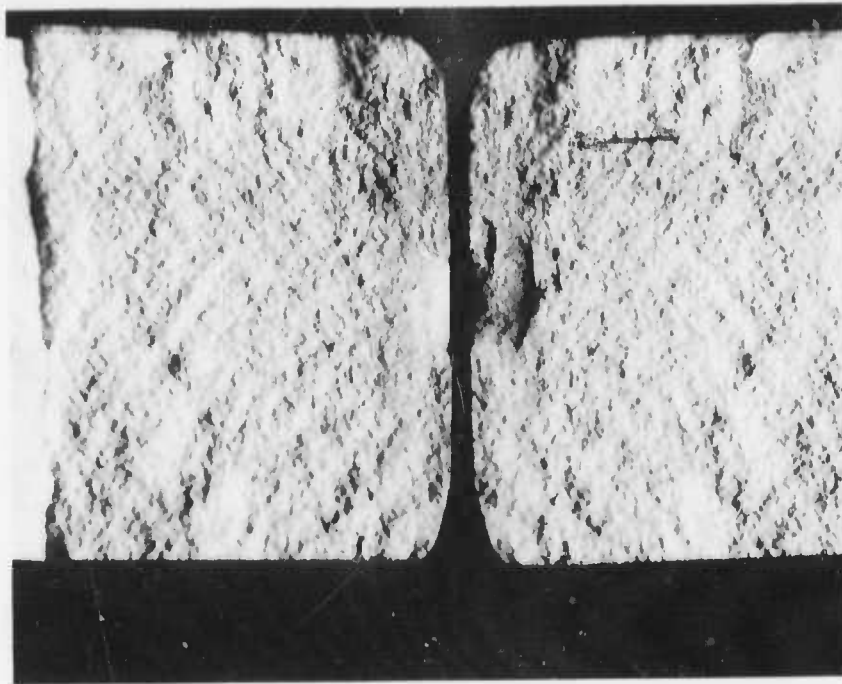


(a)

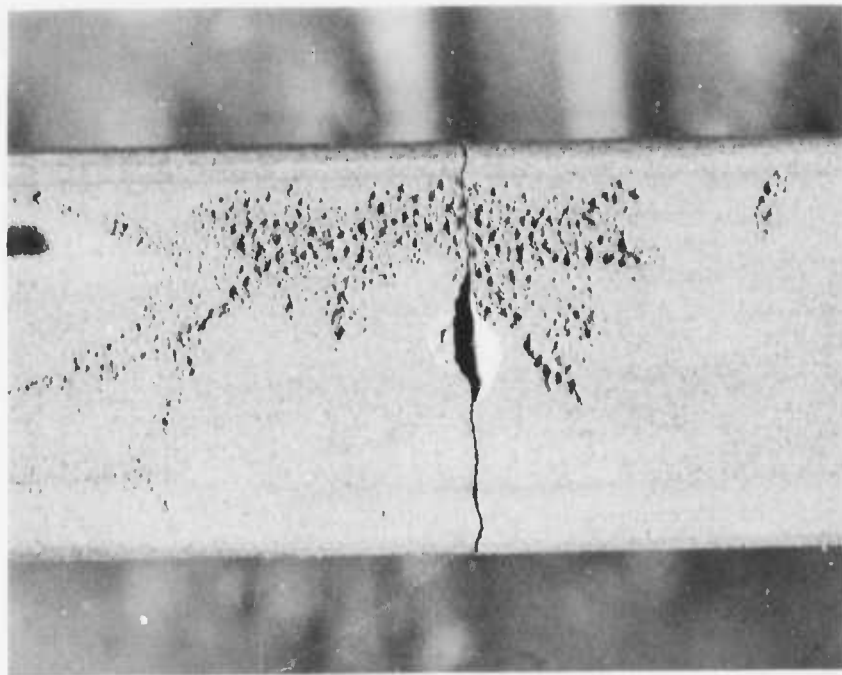


(b)

Figure 12. Fracture surface (a) and tensile surface (b) of flexure bar 3-4B.

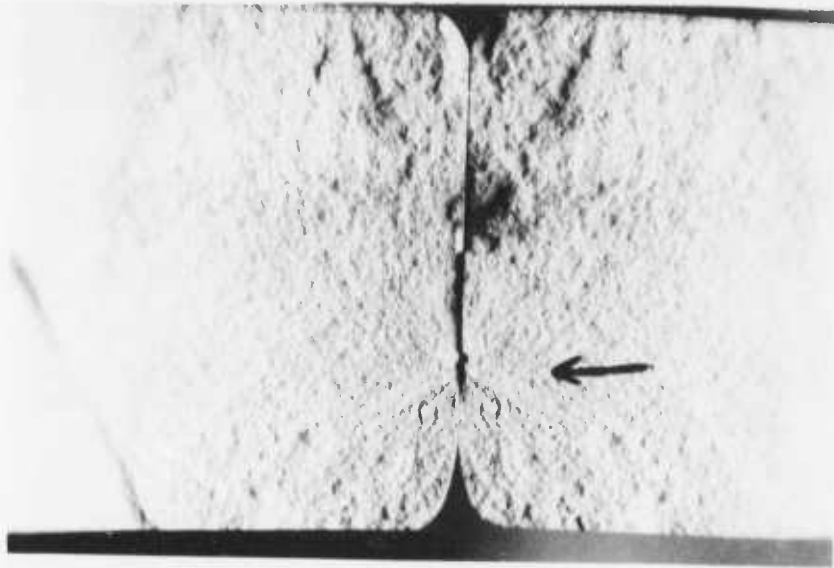


(a)

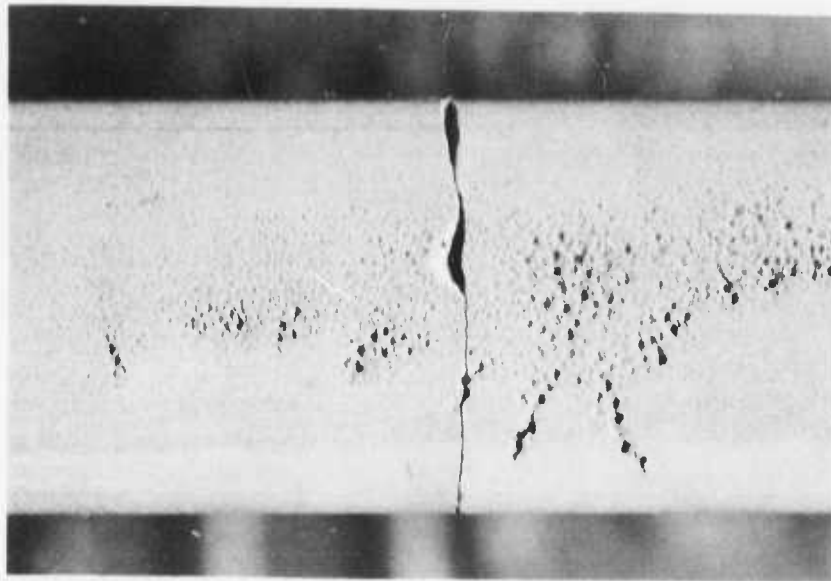


(b)

Figure 13. Fracture surface (a) and tensile surface (b) of flexure bar 3-5A.

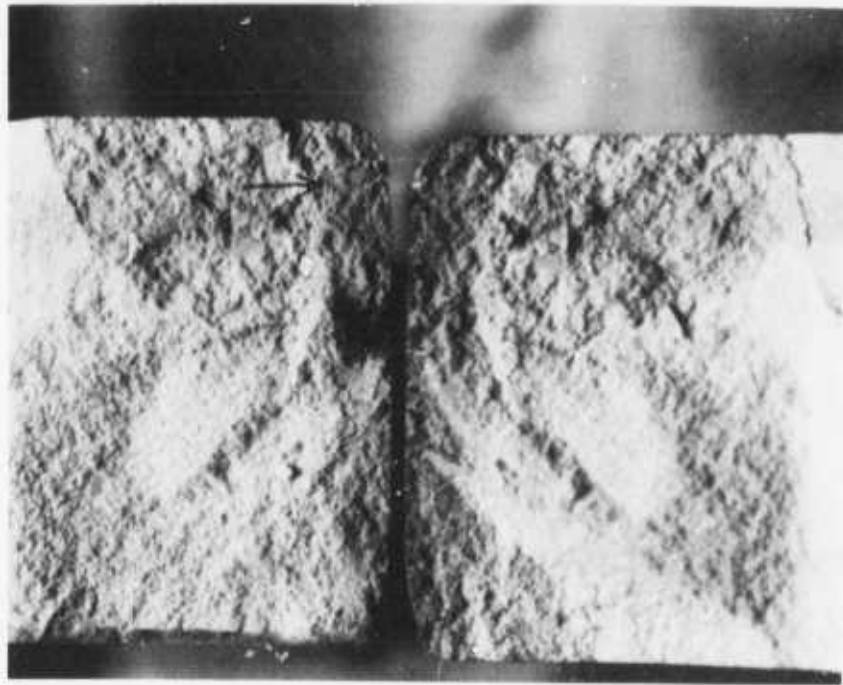


(a)

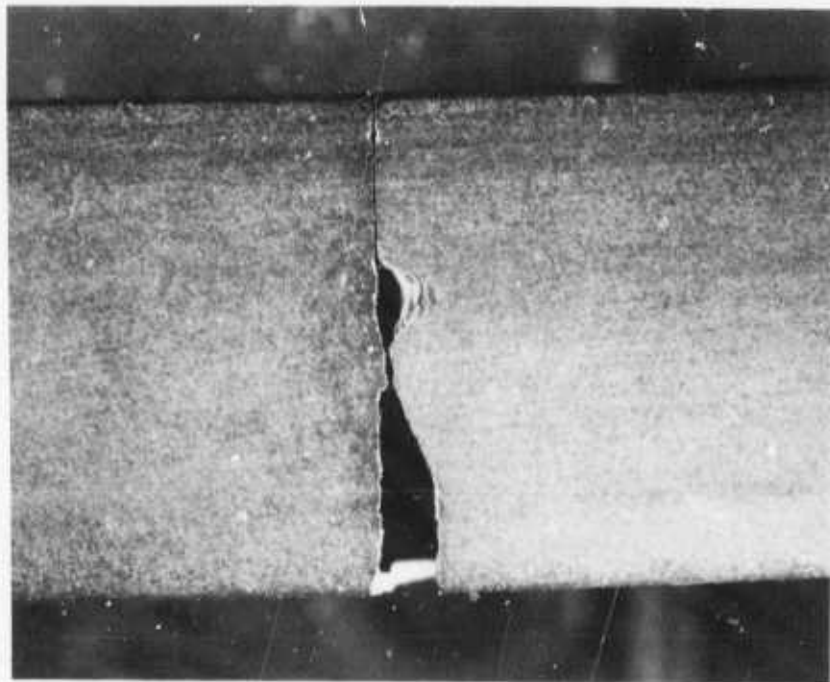


(b)

Figure 14. Fracture surface (a) and tensile surface (b) of flexure bar 3-5B.

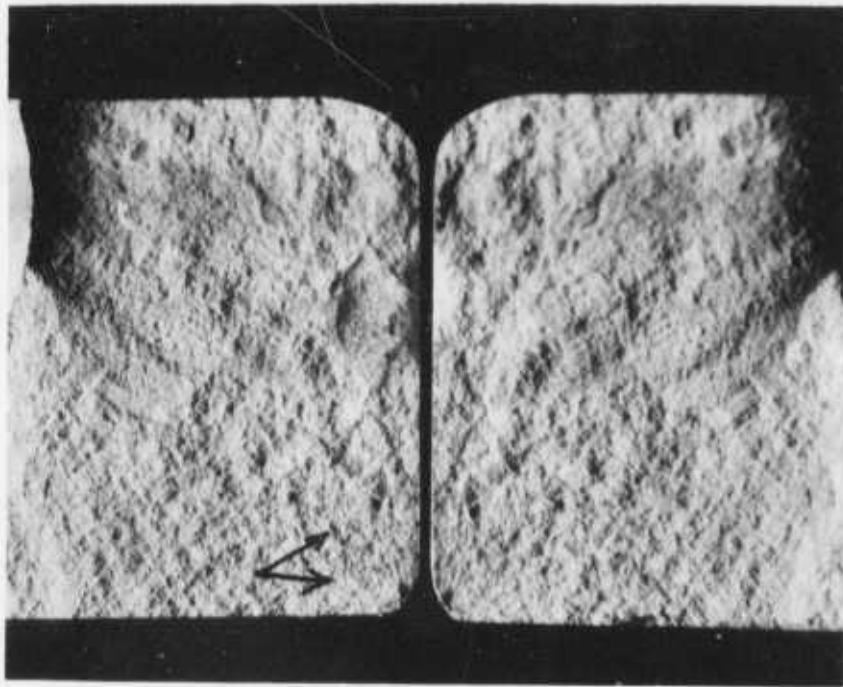


(a)

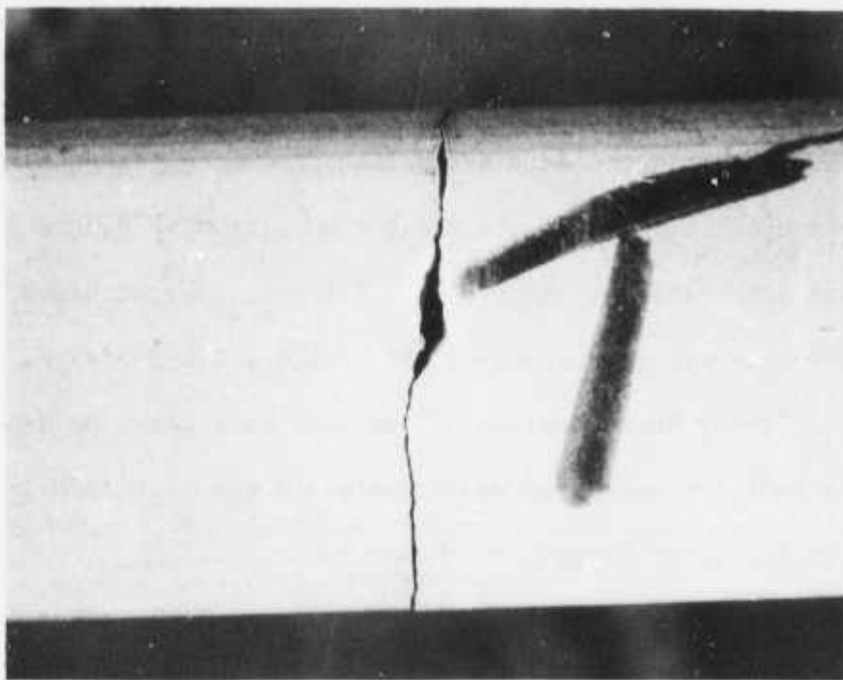


(b)

Figure 15. Fracture surface (a) and tensile surface (b) of flexure bar 5-1A.



(a)



(b)

Figure 16. Fracture surface (a) and tensile surface (b) of flexure bar 5-1B.

5. CHARACTERIZATION OF MATERIAL

a. Microstructure and Energy Dispersion Analysis by X-Rays (EDAX)

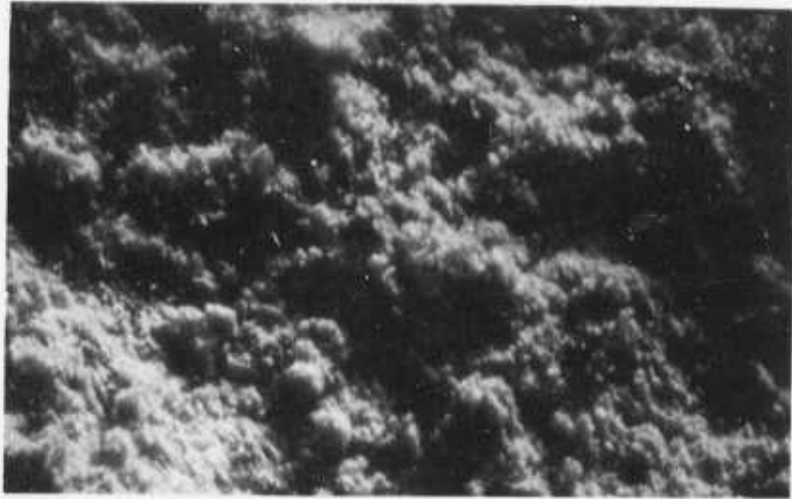
Since the radomes varied in grayness and density through the thickness and since reaction-sintered Si_3N_4 frequently fails to nitride completely in the interior, evidence for variations in Si concentration and other microstructural features was sought. The SEM micrographs of a fracture surface, Figure 17, and a polished section, Figure 18a, from Radome 3 contain no bright spots characteristic of elemental silicon. Figure 18a shows the band of porosity near the outer radome wall (top of picture). An EDAX scan of the polished sample, Figure 18b, indicates no significant difference in Si concentration with depth. An EDAX scan for impurities, Figure 19, indicates some iron, and a substantial amount of Al replacing Si, which was incorporated while the powders were milled with Al_2O_3 .

b. X-Ray Diffraction (XRD)

X-ray diffraction line intensities and data generated previously at AFML were used to estimate the phase composition of Radome 5⁴. The outer layer was approximately 59% $\alpha\text{-Si}_3\text{N}_4$, 27% $\beta\text{-Sialon}$, 6% Si_2ON_2 and 2% Al_2O_3 , while the core was approximately 69% $\alpha\text{-Si}_3\text{N}_4$, 17% $\beta\text{-Sialon}$, 11% Si_2ON_2 and 3% Al_2O_3 . X-ray determination of the unit cell size, or d-spacing, indicated that the $\beta\text{-Sialon}$ contained approximately 8 w/o $\text{Al}_2\text{O}_3 \cdot \text{AlN}$ in the core and 10 w/o in the outer layer.

c. Chemical Analysis

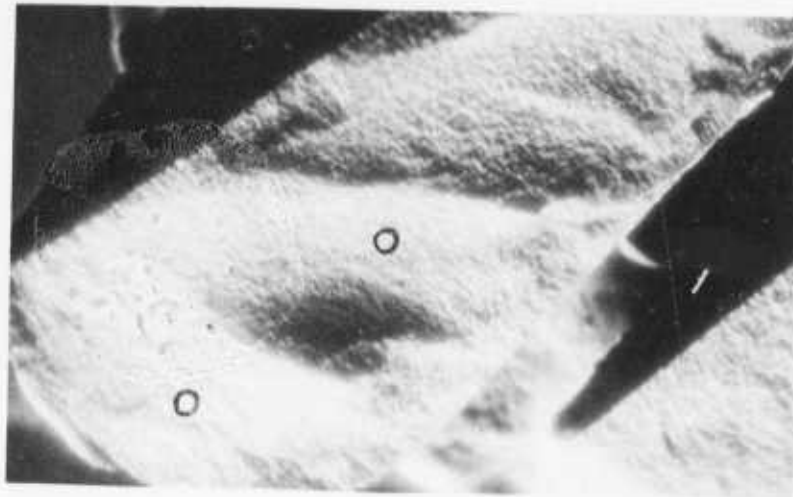
Impurity analyses for Radomes 3 and 5 are given in Table 2. The impurity levels for Radome 5 are from two different analyses and thus contains information on some elements not determined for Radome 3. The skin and bulk of Radome 5 were analyzed separately and the only appreciable



(a)



(b)

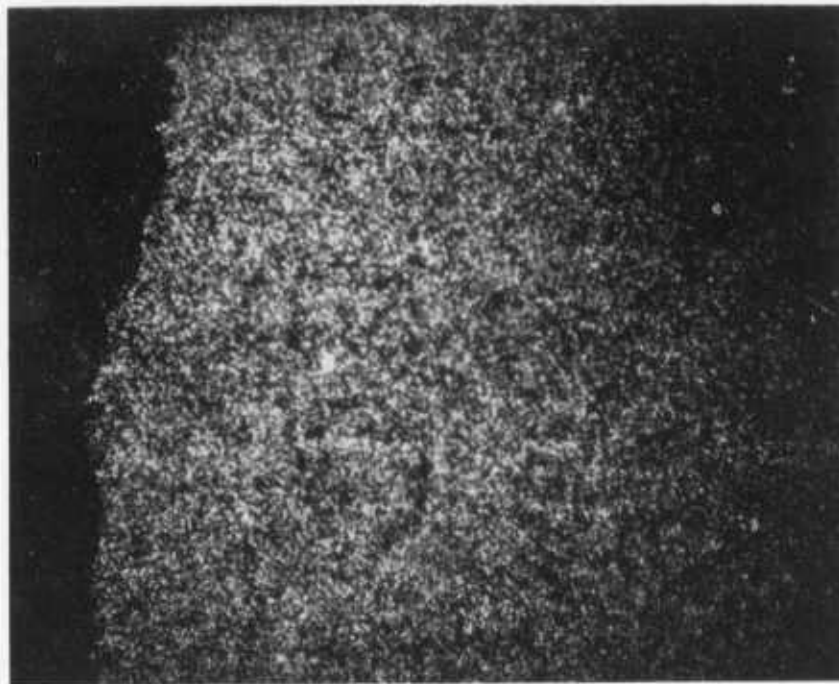


(c)

Figure 17. Secondary emission scanning electron micrographs of a sample from Radome 3. (a) 2000 X, (b) 500X, (c) 15 X. Circled areas EDAX alike.

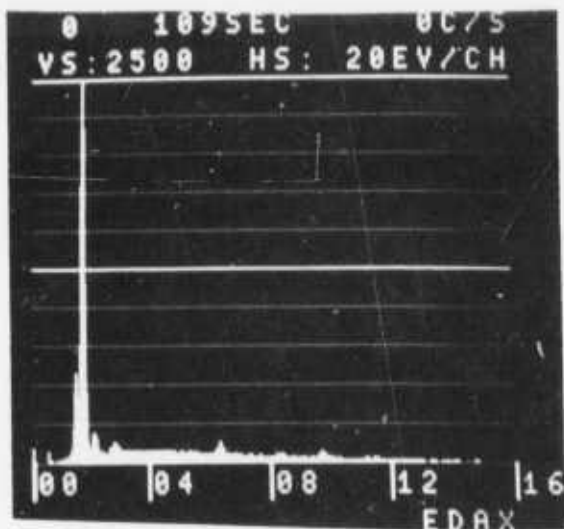


(a)

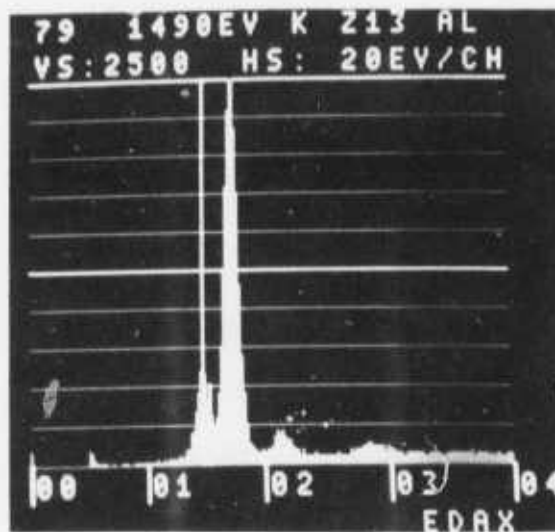


(b)

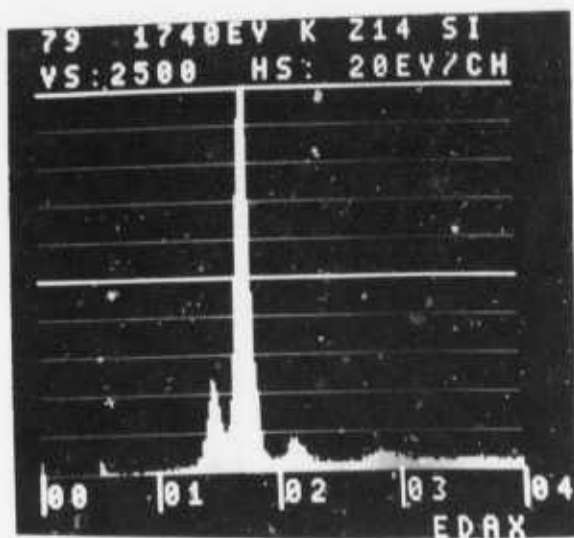
Figure 18. (a) Secondary emission scanning electron micrograph of a polished sample from Radome 3 at 20X. (b) An EDAX scan for silicon concentration in the same area.



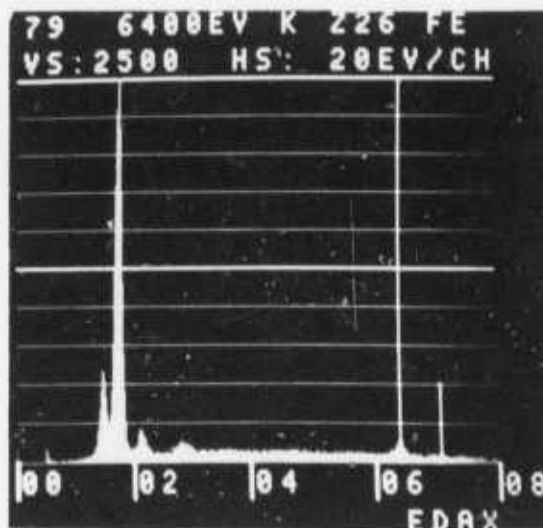
(a)



(b)



(c)



(d)

Figure 19. An EDAX trace from a polished sample of Radome 3. (a) The peaks from left to right correspond to Al, Si, Au, Pd and Fe. The Au and Pd are from the conductive coating. (b, c, d) Lines superimposed on the peaks of (a) identify the peaks belonging to Al, Si and Fe.

Table 2. Emission Spectrographic Analysis in ppm Weight

Element	Radome 3	Radome 5
B	< 20	< 20
Na	< 200	<200
Al	62,000	62,000
Fe	15,000	16,000
Mg	600	1,000
Mn	1,000	1,000
Ni	60	100
Cu	40	40
Zn	< 200	< 200
Ti	400	400
Cr	1,000	1,000
Ca	ND	1,300
Co	ND	20
Mo	< 20	< 20
Sn	<200	<200
Sr	ND	30
V	400	400
La	1,000	1,000
Zr	400	600
Pb	<200	<200
Y	ND	500

ND - Not Determined

difference was that the Zr level in the skin was 1,500 vs 600 ppm weight in the interior. The levels of Al and Fe were obtained by atomic absorption analysis. The aluminum level is about 10 w/o. The Raytheon report indicates that the Al level was <1% for dry milled powder, pages 9 and 40 but that result was subsequently found to be in error by Waugh, et.al.

d. Discussion

The Raytheon radomes are composed of 4 phases in the Si-Al-O-N system⁴. The relationship of these phases to the mechanical and dielectric properties are unknown. The impurity content is moderately high and would be expected to degrade the dielectric properties. There was no significant difference in impurity analyses for the two radomes studied.

SECTION III

CONCLUSIONS AND RECOMMENDATIONS

The measured fracture stress for the radome material ranged from 12 to 18 Kpsi, which is weak for reaction-bonded Si_3N_4 . The identifiable critical flaws in the bend bars had major and minor diameters in the range 100 to 200 microns. The corresponding dimensions of the flaws revealed by the radome fracture during CO_2 laser testing ranged from 500 microns upward. These facts suggest that radome failures could have initiated at stress levels below 8,000 psi. Clearly methods of eliminating large flawed regions is essential to the manufacture of radomes.

The radome fractures are elliptical sections through the dome wall and the fracture inclination tends to be predominantly outward from the normal to the outer surface, especially nearest the base. Fractures could have initiated from within or near the edge of the heated region. In the latter case, the large flaws which were revealed by fracture are possible sites of catastrophic fracture initiation.

The existing mathematical models of radome fracture have dealt primarily with fracture initiation from stress under the hot spot or from hoop stress outside the heated region⁵⁻⁸. There has been no specific consideration of failure arising from shear stress near the boundary to the heated region. To anticipate the correct fracture mode is important since properties may be tailored to improve performance. For example, the time to reach a given stress level may decrease with increased thermal diffusivity under the hot zone and increase near the edge of the hot zone.

The mathematical models most appropriate to the fracture of these radomes are the finite element discs used by Martin Marietta Corporation⁹. As indicated in the appendix, that work would be more useful if the stress matrices were diagonalized to yield the principal stresses and the locus

of maximum tensile stress versus time. Another factor that should be considered is the possibility that crack growth under the hot spot may be limited by stress relief and that fracture times may depend on the growth rate of the stress in more than one region and on the alternation of stress patterns from localized cracking.

SECTION IV

REFERENCES

1. R.W. Rice, R.C. Pohanka, and L. Churk, "Strength Size Effects in Ceramics," Bull. Am. Ceram. Soc 56 (3), 296 (March 1977).
2. G.K. Bansal, W.H. Duckworth, and D.E. Niesz, "Strength Size Relations in Two Hot-Pressed Ceramics," Bull. Am. Ceram. Soc. 56 (3), 296 (March 1977).
3. J.S. Waugh and M.M. Jaremchuk, "Reaction Sintered Silicon Nitride Material Optimization for Radome Applications, "AFML Technical Report No. AFML-TR-76-182 (Raytheon Research Division, Waltham, Mass., 1976).
4. P.L. Land, J.M. Wimmer, R.W. Burns, and N.S. Chondhury, "Compounds and Properties of the Sialon System." AFML-TR-75-209, April (1976).
5. W.T. Laughlin, "Predicting the Laser Induced Thermal Fracture of Infrared and Radar-Transmitting Materials," Proceedings of the 1st DOD Conf. on High Energy Laser Technology, pp. 627-47 Oct. 1974, San Diego, Calif. (CONFIDENTIAL).
6. J.J. Mecholsky, R.W. Rice, and J.R. Spann, "Laser-Induced Thermal Stress Failure of Ceramics," in Proceedings of the 1973 Laser Effects/Hardening Conference: Vol. II - Thermal Effects, M73-115 (MITRE Corp.) N.F. Harmon, ed.), p. 173 (SECRET).
7. L.B. Weckesser, "Pyroceram 9606 Fracture-Test and Theory," In Proceedings of the 1973 Laser Effects/Hardening Conference: Vol. II - Thermal Effects, M73-115 (MITRE Corp.) (N.F. Harmon, Ed.) p. 179 (SECRET).
8. R.W. Rice and J.R. Spann, "The Effect of High Energy Laser Radiation on Ceramics," in NRL High Energy Laser Program Progress Report for period 15 October 1970 to 15 January 1971, NRL Memorandum Report 2222 (H.W. Gandy, D.J. McLaughlin, H. Shenker, and A.I. Schindler, eds.) (SECRET).

9. A. Ossin, "A Three Dimensional Stress Analysis on the Effects of a Laser Induced Local Hot Spot on a Silicon Nitride Shell, " Martin Marietta Corporation. Analysis Report, AFML Contract F33615-76-C-5276 (D.J. Evans, AMFL/LPJ, Contract Monitor). Unpublished.
10. S.S. Cunningham and W.T. Laughlin, "The Fracture of Full Scale Pyroceram Samples," in Proceedings of the 1973 Laser Effects/Hardening Conference: Vol. II - Thermal Effects, M73-115 (MITRE Corp.) (N.F. Harmon, ed.) p. 169 (SECRET).
11. F. Erdogan and G.C. Sih, "Crack Extension in Plates under Plane Loading and Transverse Shear," J. Basic Eng., Trans. ASME Ser. D 85, 519-27, (1963).
12. J.J. Petrovic and M.G. Mendiratta, "On Mixed Mode Fracture from Controlled Surface Flaws in Hot Pressed Si_3N_4 ," accepted for publication in J. Am. Ceram. Society.
13. J.J. Petrovic and M.G. Mendiratta, "Mixed Mode Fracture from Controlled Surface Flaws in Hot Pressed Si_3N_4 ," J. Am. Ceram. Soc. 59, 163-7 (1976).

APPENDIX A
STRESS ANALYSIS

It is probable that the catastrophic fracture of the Raytheon radomes initiated in a mode resulting from stress along an approximately conic section through the dome, near the boundary of the irradiated zone. This fracture mode is consistent with the location of the flaws exposed by the fracture, with the fact that AFWL motion pictures showed the fractured material being ejected outward into the air stream, and with the fact that the fracture did not radiate outward as might be expected from tensile stress directly beneath the heated surface,* or from hoop stress in the material outside the heated area.

Previous work on fracture of ceramics under CO₂ laser flux⁵⁻⁹ does not specifically address the mode of failure which is suspected to have occurred in these radomes and in other test specimens⁸ and radomes¹⁰. The well known papers by Laughlin⁵ and by Mecholsky, et al.,⁶ which address failure resulting from stress in the interior or near the back surface of an opaque material, utilize one-dimensional models for which stress varies with depth only. The stress and momentum imparted with fracture are in a plane parallelling the sample surface. Application of these models is restricted to cases where the beam size is large compared to the sample thickness. Weckesser⁷ has used a two-dimensional analysis of radome failures, but he did not discuss the mode of failure considered here.

*Fracture causes transient stress which can cause a crack to tend to extend on a tangent surface rather than on the surface associated with the maximum prefracture stress.

The most recent analysis and the one considered most relevant to the fracture of the Raytheon radomes was performed by Martin Marietta Corporation under AFML/OPJ Contract F33615-76-C-5276 monitored by D.J. Evans⁹. Three-dimensional, axially symmetric, finite-element thermal-stress models were used to study the stress generated by uniform laser-induced hot spots on curved and flat discs of silicon nitride. The disc models were 3 inches in diameter and 0.3 inches thick, with either free or fixed edges*. The beam diameters were 1.2, 2.4, and 4 cm. The stresses are described as radial, hoop, shear and axial. The report indicates that the analysis predicted failures from tension in the midsection under the hot spot, hoop tension outside the hot spot, and shear stress in the heated zone, and that all types of failure are corroborated by evidence from motion pictures of tests on discs.

It is generally agreed that the fracture of a ceramic having homogeneous mechanical properties and a uniform flaw distribution will almost always initiate on a surface that is subjected to the maximum tensile stress^{11**}. Therefore, it is logical to diagonalize the stress matrices in order to determine the axially-symmetric locus of maximum tensile stress at selected times. Following initiation, a fracture will tend to follow the surface of maximum thermally induced stress, but the path will also be effected by the transient stress produced by the fracture process and by inhomogenities in the path of the advancing crack front. In some cases it is expected that

* Although not stated by Ossin, et al, these boundary conditions are extremes and bracket the realistic case.

** In cases where only a few large flaws limit strength, it is not permissible to assume that the maximum tensile stress will be oriented normal to the weakest plane of cohesion through a flaw, as one can when a large number of flaws are present. In such cases the principal of maximum strain energy release rate may be more appropriate than the principal of maximum stress^{12,13}.

crack growth in a region of maximum tensile stress may be limited by stress relief, and a subsequent increase in stress in another region may cause the ultimate catastrophic fracture.

The Martin Marietta (M.M.) model most appropriate to consideration of stress in the Raytheon radomes are those for a 4-cm-diameter hot spot on a spherical disc with fixed edges. The axial stress curves are not given for this configuration so the stress curves for a 2.4-cm-diameter hot spot, pages 31,37 and 40, were used to calculate the principal tensile stress at selected points in the disc. The stress matrix for the model, which contains only 3 independent stresses, is defined by Figure A-1.

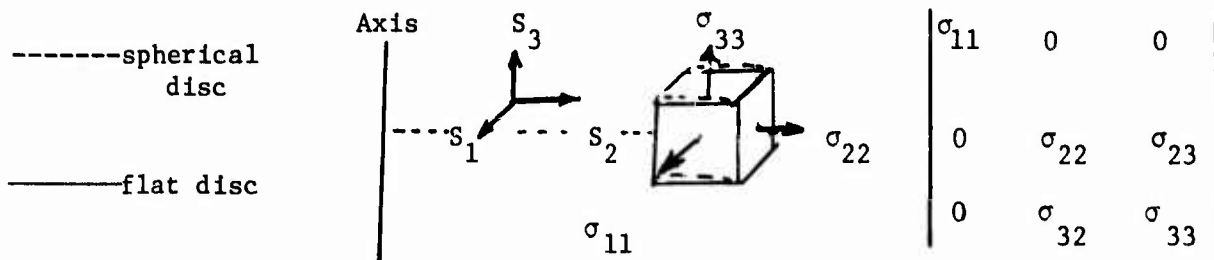


Figure A-1.

Solving the determinate

$$\begin{vmatrix} A & -\lambda \end{vmatrix} = 0, \text{ where } A = \begin{pmatrix} \sigma_{22} & \sigma_{23} \\ \sigma_{32} & \sigma_{33} \end{pmatrix}$$

yields the magnitude of the principal stresses,

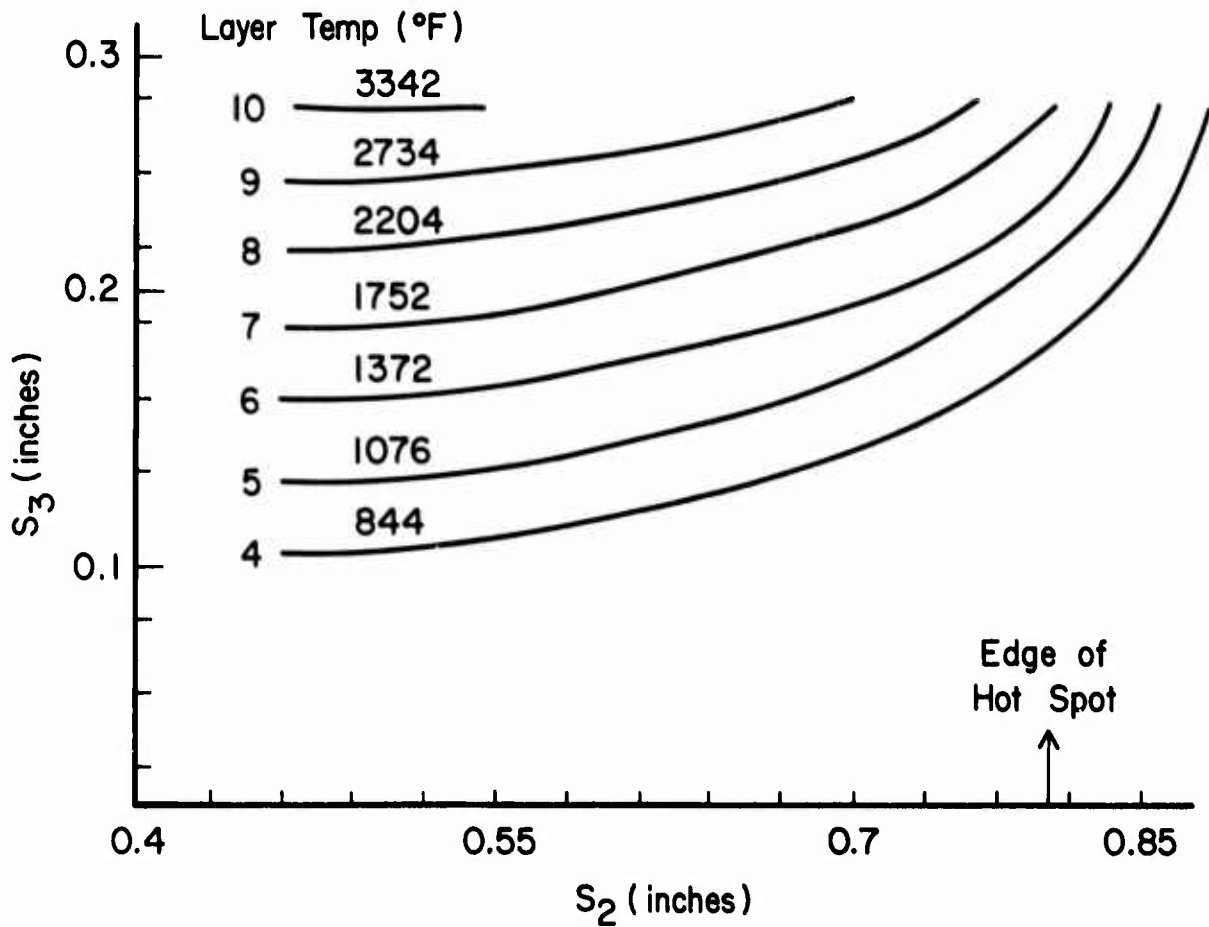
$$\lambda = 1/2[\sigma_{22} + \sigma_{33} \pm [(\sigma_{22} - \sigma_{33})^2 - 4(\sigma_{22}\sigma_{33} - \sigma_{23}^2)]^{1/2}]$$

Hoop is already a principal stress. The + sign yields the largest principal tensile stress which is the stress of primary interest. For the curves on pages 31, 37 and 40, the principal stress at points located 0.2 inches from the disc center on sheets 1, 6 and 10, respectively are 8, 33, and 28 Ksi, and the corresponding principal directions are (0,0.3,1,) (0,1,0.09) and (0,0.4,1) using the unit vector directions of Figure A-1. In these examples and throughout the disc, the maximum principal stress direction is inclined

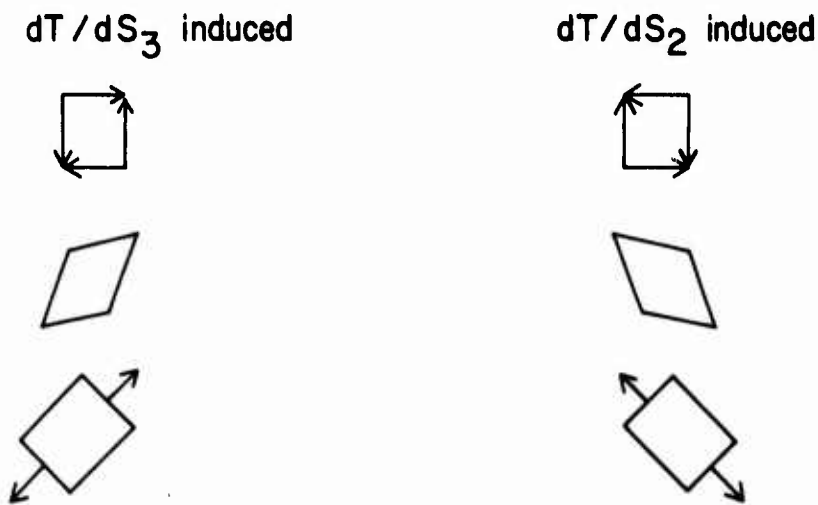
upward and outward (positive S_2 and S_3). The fracture surfaces for tensile failure are inclined at 90° to the principal stress and the momentum imparted to fragments would be generally downward ($-S_3$), if it is assumed that the top surface is irradiated.. Figure A-2 shows isotherms in a model disc of Si_3N_4 after 2 seconds of heating and also the limits of shear stress occurring as a result of the temperature gradients. The stress developed by dT/dS_3 (which is plotted as a positive shear by Martin Marietta) is shown at the left together with the corresponding shear strain and the equivalent tensile strain. The shear stress resulting from dT/dS_2 is the inverse of that resulting from dT/dS_3 . The latter is shown on the right along with the corresponding shear strain and equivalent tensile strain. A temperature gradient at 45° to the disc surface causes a locally produced shear that is equivalent to a tensile stress in the S_3 direction.

The Martin Marietta curves for shear versus S_2 are positive everywhere. Since there are regions outside the heated spot where $dT/dS_2 > dT/dS_3$, as shown in Figure A-2, it is presumed that remotely generated stress accounts for the shear being positive near and outside the boundary of the heated region. The consequences of the shear stress being positive everywhere is that the principal tensile stress in any volume element has S_2 and S_3 components with the same sign. Fracture resulting from this tensile stress would initiate on an orthogonal surface having a "negative" inclination. This does not account for fragmentation momentum in the S_3 direction.

It may be that some tensile fractures initiating between zones of compression within a heated region propagate to a limited extent only. If so, this precatastrophic cracking could cause a substantial and rapid increase in the hoop stress in regions further from the disc center; similarly it could cause changes in the stress near the boundary of the heated region



(a)



(b)

Figure A-2. (a) The isotherms for a 0.3 inch thick disc of Si_3N_4 with a 1.56 inch diameter hot spot applied for 2.0 seconds as calculated from MM Figure 35. (b) The limits of locally induced shear stress and shear strain for the above figure and the equivalent tensile stress-strain.

that could contribute to catastrophic fracture on a surface of "positive" inclination.

The concept of precatastrophic cracking as discussed above has not been addressed before. If it does occur, it might be detected by acoustic emission sensors attached to laser test samples. Of course acoustic emission could be associated with both precracking and failure at a single site as well as with precracking and failure at separate sites, so one would need to differentiate between these possibilities before involving this kind of precatastrophic cracking in a mathematical model.

**THIS REPORT HAS BEEN DELIMITED
AND CLEANED FOR PUBLIC RELEASE
UNDER DOD DIRECTIVE 5200.20 AND
NO RESTRICTIONS ARE IMPOSED UPON
ITS USE AND DISCLOSURE.**

DISTRIBUTION STATEMENT A

**APPROVED FOR PUBLIC RELEASE,
DISTRIBUTION UNLIMITED.**